Spectral Entropy as a marker for the laminar-turbulent transition. An experimental used-case with high-speed PIV measurements in a helically coiled reactor.

Conrad Müller*, Péter Kováts, Katharina Zähringer

Lehrstuhl für Strömungsmechanik und Strömungstechnik
Otto-von-Guericke-Universität Magdeburg
39106 Magdeburg, Germany
*conrad.mueller@ovgu.de

ABSTRACT

Helically coiled reactors (HCRs) or short helix reactors play an important role in industrial applications concerning heat and mass transfer and static mixing. They provide a simple geometry with low pressure losses and maintenance costs compared to other mixing processes. The impact of the most important geometrical parameters, the torsion, the pitch and curvature ratio are well researched. However, the laminar-turbulent transition in helically coiled reactors is still very divided as shown in Figure 1.

The aim of this work is to validate the spectral entropy as a maker for the laminar-turbulent transition by comparing it to traditional markers and visualizations (Müller et al., 2026). The spectral entropy correlates over the whole measurement area and time. The resulting transition marker is therefore, once validated, independent of time and space and applicable to any given geometry independent of its complexity. It is also more comprehensive compared to traditional markers like the turbulence intensity. It is applied here to the optically measured velocity fields in three transparent helically coiled reactors with three different curvature ratios to determine their laminar-turbulent transition.

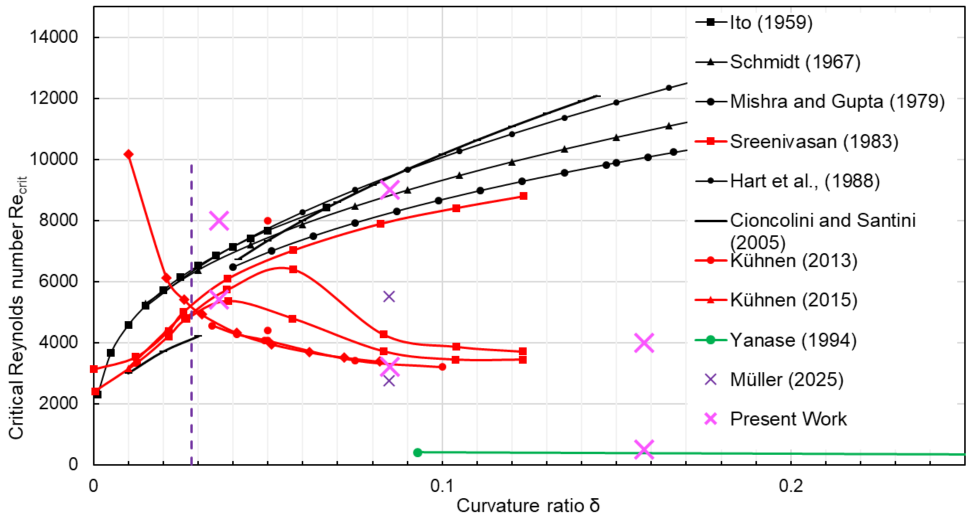

Figure 1: Laminar-turbulent transition from selected literature marked by the critical Reynolds number as function of the curvature ratio of helix reactors and tori. Black curves are related to pressure measurements and red curves are related to velocity measurements, green curves are numerical results and pink shows the upper and lower boundary of the transition resulting from the present paper.

INTRODUCTION

Helically coiled reactors (HCRs), also referred to as helix reactors, have been investigated for more than a century (Eustice, 1910, 1911) due to their industrial relevance, particularly their ability to enhance static mixing and heat and mass transfer while maintaining low pressure drop and maintenance costs (Vashisth et al., 2008). With the development of newer coiled geometries such as the coiled flow inverter (CFI, Mandal et al. (2011)), the coiled flow reverser (CFR; Mansour et al. (2023)) and even more complex configurations (Li et al., 2025), renewed attention has been directed towards a fundamental understanding of the simple helix reactor.

Most experimental and numerical studies in the literature focus on single-phase liquid–liquid mixing, investigating concentration fields, flow structures and pressure drop behaviour. In addition, heat and mass transfer in HCRs has been extensively studied both experimentally and numerically. The influence of key dimensionless numbers, namely the Reynolds, Dean and Schmidt numbers, as well as geometric parameters such as the curvature ratio $\delta = d_i/D$, pitch p and torsion τ, has been widely analysed. While pitch and torsion were found to have only minor effects on the flow, the curvature ratio emerges as the dominant geometric parameter. These governing factors have also been addressed in numerical optimization studies. Furthermore, multiphase investigations have examined gas–liquid mass transfer and flow regime characteristics. Comprehensive overviews of HCR research are provided in recent reviews by Sigalotti et al. (2023), building upon earlier reviews by Naphon et al. (2006) and Itó (1987).

A key aspect of flow behaviour in HCRs is the transition from laminar to turbulent regimes, which strongly affects mixing, heat and mass transfer, and pressure loss. In contrast to straight tubes, where transition typically occurs at $Re \approx 2300$, reported critical Reynolds numbers in helical reactors span a wide range. This shift is often attributed to re-laminarizing effects (Narasimha et al., 1979) induced by curvature. However, variations in geometric configurations, measurement techniques and flow asymmetries caused by centrifugal forces and Dean vortices complicate the interpretation of transitional flow behaviour in helix reactors, leading to the discrepancies in Figure 1.

In this work, the laminar-turbulent transition is measured with high-speed particle image velocimetry (PIV). The resulting vector fields are analysed with traditional markers and the Spectral Entropy Method is validated as innovative alternative to characterize the laminar-turbulent transition of experimental data.

EXPERIMENTAL SETUP

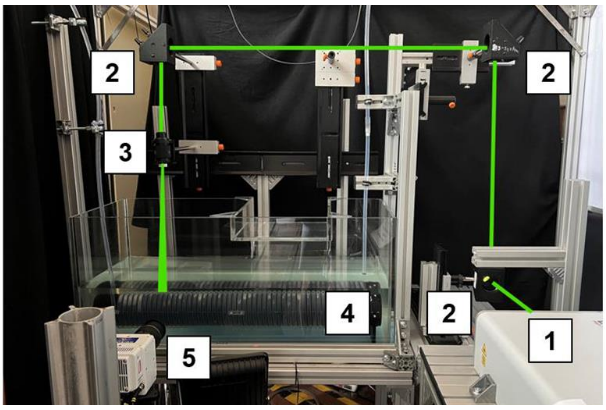

Figure 2: PIV setup with helix reactor in the acrylic glass tank filled with refractive index matching solution and laser path visualized in green. Numbers are explained in the text. (Müller et al., 2026)

Figure 2 shows the experimental setup which was established in Müller et al. (2025). The transparent helix reactors are made from Fluorinated Ethylene Propylene (FEP) with an inner diameter of $\boldsymbol{d_i}$ = 6 mm, a wall thickness of 1 mm. Three different helix reactors with three coil diameters D and from that resulting curvature ratios $\delta = \frac{\boldsymbol{d_i}}{\boldsymbol{D}}$ = 0.158, 0.085 and 0.036 were measured. Due to the high amount of results only a selected range of the measurements taken in the top cross-section of the 6th coil will be shown in this paper, covering the most important findings.

They are fed by a gravity driven flow and the flow rates are set by a needle valve and measured with an ultrasonic flow meter. For refractive index matching, the helix reactor is placed in an aquarium [4] filled with a 5.25%vol. glycerol-water solution. The same solution is used as working fluid inside the reactor tubes. The PIV setup to measure the velocity fields inside the helix consists of a high-speed laser [1], several mirrors [2] leading the laser beam to a light sheet optic [3], and a Phantom VEO L640 high-speed camera [5]. As tracer particles silver coated hollow glass spheres with 10 µm diameter are used. The volume flow rate is set between 0.18 and 3.86 l/min to achieve a range of Reynolds numbers between Re = 500…11000 covering the expected transition range from Figure 1, resulting in a total amount of 108 radial measurements. The recording frequency is set according to the pixel shift between 0.2 and 10 kHz.

PROCESSING

The image processing follows the established practice of Müller et al. (2026). In addition, the Spectral Entropy Method (Abdelsamie et al., 2017) combines the temporal and spatial aspects of the flow and is added as marker for transition providing a more universal consideration.

Velocity field calculation

After a geometrical calibration, only a sliding gauss filter is subtracted as pre-processing of the raw PIV images. A multi-pass cross-correlation with interrogation windows of 64x64 and 32x32 pixels with 50% overlap is used to calculate the vector fields with the software DaVis from LaVision GmbH. As further vector treatment only a median filter is used, avoiding strong smoothing filters, but also filling up empty spaces in the vector grid, which would lead to problems in later analytical steps.

Pseudo-3D-visualization

The 2D-vector fields of the cross-sectional measurements are combined in DaVis forming a pseudo-3D representation with the recording frequency normalized by the superficial flow velocity as pseudo axial coordinate between two consecutive snapshots. To visualize vortex structures the Q-criterion is represented as iso-surface. Since the overall vorticity increases with rising Reynolds number, in the visualizations the dimensionless Q-criterion $Q*$, normalized with the superficial flow rate and the inner diameter of the tube, is kept at a constant value of $\boldsymbol{Q^*} = \mathbf{2 \cdot 10^{-7}}$ for all cases.

$$Q^* = \frac{Q \cdot d_i^2}{u_s^2} = \frac{Q \cdot d_i^6 \cdot \pi^2}{\dot{V}^2 \cdot 16} \tag{1}$$

The Q-criterion threshold set in the pseudo-3D-visualization results to $Q = 0.0001\ldots0.0288$ 1/s². Further detailed explanations of this post-processing process can be found in Müller et al. (2026). The transition is determined qualitatively by the secondary vortex occurrence additionally to the Dean vortices.

Turbulence parameters

From the 2D flow fields, at specific points of interest, velocity as function of time signals are extracted. Of those signals the turbulence intensity (TI) is calculated (Eq. 2):

$$TI = \frac{u'_{rms}}{\bar{u}} \cdot 100\% = \frac{\sigma}{\bar{u}} \cdot 100\% \tag{2}$$

Further, the dissipation rate is calculated for two dimensions (Eq. 3) with approximated velocity gradients (Eq. 4). The dissipation rate is then averaged over the time of one measurement series and also spatially over the whole measurement area:

$$\langle\overline{\varepsilon_{2D}}\rangle = \frac{1}{N \cdot t_{total}} \sum_{t_{steps}} \sum_{x_i, y_i} 2\nu \left[\left(\frac{\partial u}{\partial x}\right)^2 + \left(\frac{\partial v}{\partial y}\right)^2 + \frac{1}{2}\left(\frac{\partial u}{\partial y} + \frac{\partial v}{\partial x}\right)^2 \right] \tag{3}$$

with

$$\frac{\partial u}{\partial x} \approx \frac{u(x + \Delta x) - u(x - \Delta x)}{2\Delta x} \tag{4}$$

The size of the smallest structures within the flow can be estimated from the dissipation rate and the viscosity by the Kolmogorov length scale $\boldsymbol{\eta}$ (Pope, 2000) and time scale $\boldsymbol{\tau_\eta}$:

$$\eta = \left(\frac{\nu^3}{\varepsilon}\right)^{1/4} \quad ; \quad \tau_\eta = \left(\frac{\nu}{\varepsilon}\right)^{1/2} = \frac{\eta^2}{\nu} \tag{5; 6}$$

Power Spectral Density analysis (PSD)

For the frequency analysis of the flow a PSD according to Welch is used. The resulting spectrum in function of the normalized frequency (Strouhal number), is to be shown in a log-log diagram and compared to the Kolmogorov slope of $-5/3$ representing the energy dissipation in fully developed, homogenous turbulence (Pope, 2000) and against the Kraichnan (or enstrophy) slope of $-10/3$ (Kraichnan et al., 1980), which is used for 2D turbulence or flows with a high helicity.

Spectral Entropy

The spectral entropy is used as novel marker regarding the laminar-turbulent transition for experimental data. It was originally designed and used for DNS simulations (Abdelsamie et al., 2017). It is able to capture the time dependency of turbulence as well as the spatial differences of the asymmetrical flow field in the helix reactor. Spectral entropy values of laminar flows are much smaller than for turbulent flows. In the transition region a strong slope can be found relating the values for laminar and turbulent conditions.

Spectral entropy uses the fundamental idea of the POD and decomposes the flow field signal into orthogonal deterministic functions (spatial modes, M) and time dependent coefficients. A detailed explanation of the calculation of the spectral entropy can be found in Abdelsamie et al. (2017). Most importantly, an eigenvector problem is solved leading to an amount of eigenvalues and eigenvectors equal to the amount of input snapshots. Then the relative energy P^l of each mode is calculated and sorted by intensity. The first mode then represents the average flow field. The sum of all mode's energy resembles the spectral entropy (Eq. 7):

$$S_d = -\sum_{l=1}^{M} P^l \ln P^l \qquad (7)$$

In the case of a laminar flow, only the first mode contains all energy, for which the spectral entropy becomes 0. In a fully turbulent case the energy is divided equally over all modes and all eigenvalues are equal.

The input snapshot matrix contains the flattened velocity vector. Measured and analysed are here only the single radial vector components u and v, and both together as u-v plane, as well as the vector magnitude $\|\boldsymbol{u}\|$.

In order to arrange the input data, a scale approximation is done using the Kolmogorov time and length scales, to assure independency of the input snapshots. Even though, turbulence is always a three-dimensional problem, in the following all measured velocity components and combinations are tested individually to analyse its individual influence on the spectral entropy.

RESULTS

Pseudo-3D-visualization

Figure 3 visualizes vortex structures using the Q-criterion represented as iso-surface coloured by the z-vorticity in a top down view of the pseudo-3D-visualization. For the lowest curvature ratio of δ = 0.036 at lower Reynolds numbers only the two Dean vortices are present (blue and red lines). Starting at Re = 5400 secondary vortex structures occur, which are permanently existing from Re = 8000 onwards. With bigger curvature ratios, the first onset of secondary vortex structures happens at Re = 3200 for δ = 0.085 and at Re = 500 or even before for δ = 0.158. Those secondary vortex structures occur in the outer region of the tube's cross-section with dependency on the curvature ratio. The bigger the curvature ratio, the stronger are the radial forces pushing the liquid against the outer tube wall. While for the strongest curvature the secondary vortices occur only in the outer half, for the weakest investigated curvature these vortices appear almost in the centre of the cross-section. This onset of additional vortex structures, different from the laminar flow regime, can be considered as lower boundary of the transition region. When the secondary vortices are permanently present and Dean vortices alone do not exist anymore, that state is used as upper boundary for the transition region. These visualizations are used as basis to validate the numerical markers later. In the following, we will call "laminar", "transitional" and "turbulent" regions based on these qualitative results and corresponding Reynolds number ranges.

Turbulence Intensity

In comparison to the turbulence intensity in a straight tube, the axial turbulence intensity in helix reactors is lower due to the re-laminarization. However, the turbulence intensity of the radial velocity components, as measured with our PIV setup, is much higher due to the dominant Dean vortices.

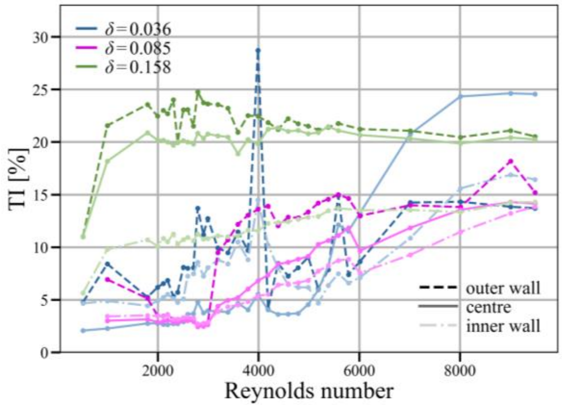

Figure 4: Turbulence Intensity at different positions extracted from the cross-sectional flow fields measured with PIV.

The first change of TI happens with the onset of secondary vortices (Figure 4). For the reactor with a curvature ratio of δ = 0.036 this onset Reynolds number is Re = 5400, as soon as secondary vortex structures occur. With rising curvature ratio, this onset shifts to lower Reynolds numbers, being Re = 3200 for δ = 0.085 and Re = 500 for δ = 0.158, where for the later secondary vortices are already present. After the initial onset, the shape of the TI curve depends on the position in the cross-section. For δ = 0.158 the TI starts dropping, similar to the trend in a straight tube, but in the inner section of the tube the TI increases further until it reaches its maximum plateau at Re = 6000. The same is true for δ = 0.085, where the outer position reaches the maximum TI at Re = 5000, while the lower positions only reach a maximum plateau at Re = 10000. For the lowest curvature ratio of δ = 0.036, which is closest to the straight tube, the centre has the highest TI vales, corresponding to the position of the secondary vortex structures which don't get pushed outwards so strongly. Since the flow profile is less deformed, the different positions reach their plateau together at Re = 8000.

Power Spectral Density

Figure 3 shows the energy spectra as function of the dimensionless frequency (Strouhal number) exemplarily for the helix with curvature ratio δ = 0.085. Laminar velocity signals show a flat line and fully developed turbulence appears as a -5/3 and -10/3 slope. Even though the laminar flow state and the transition between the two states is not clearly defined, the differences are clearly visible. The first Reynolds number different from the laminar flow conditions is Re = 3200. With increasing Re, the slope of the energy spectra increases. From Re = 8000 the slopes are not further changing, revealing the significant -5/3 slope which then shifts to a -10/3 slope at higher Strouhal numbers.

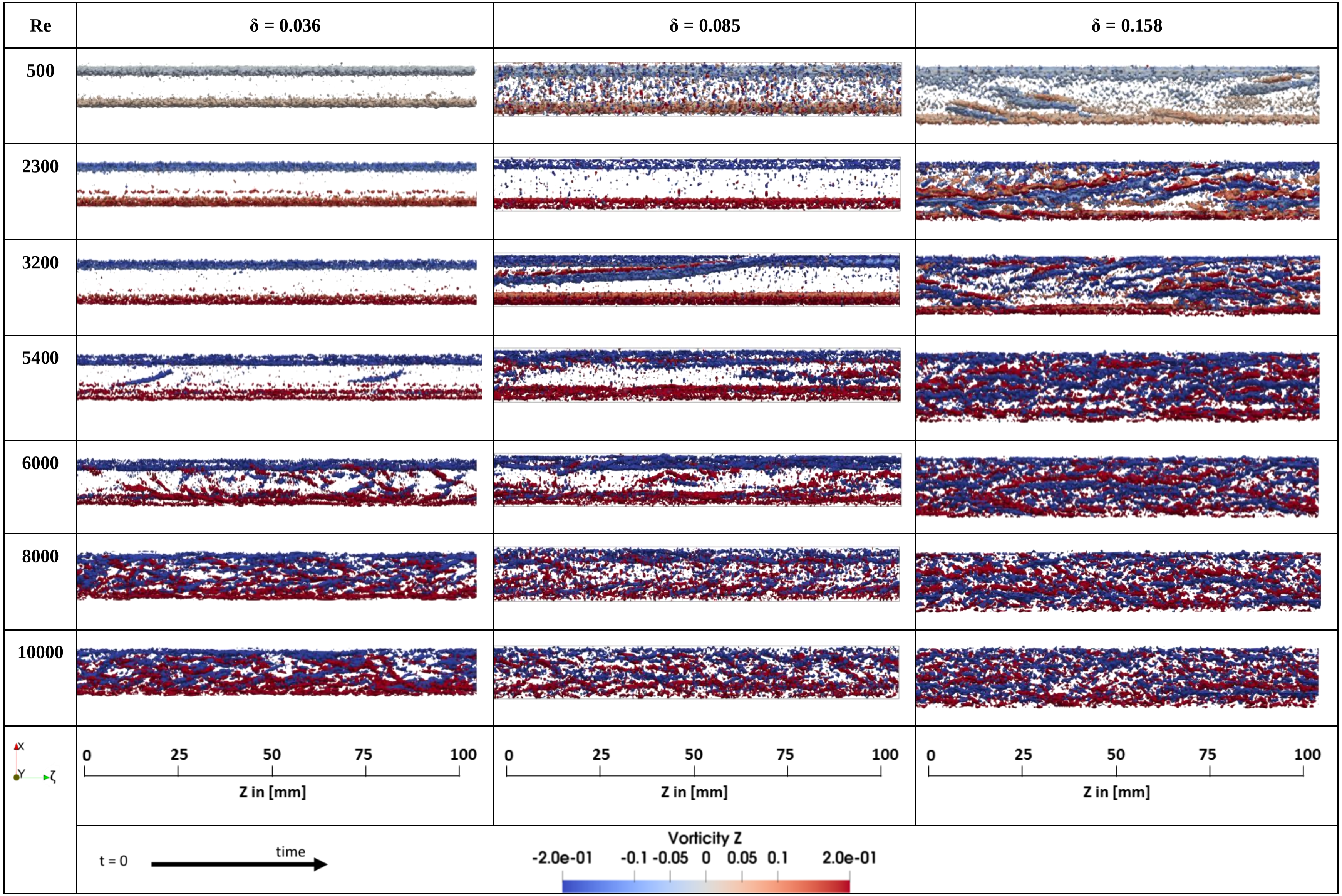

Figure 3: Representations of the flow fields for δ = 0.036; 0.085 and 0.158 (from left to right) for selected Reynolds numbers in a top down view of the pseudo-3D-visualizations. Isosurface of Q-Criterion coloured with z-vorticity. Dimensionless Q-criterion $\boldsymbol{Q^* = 2 \cdot 10^{-7}}$.

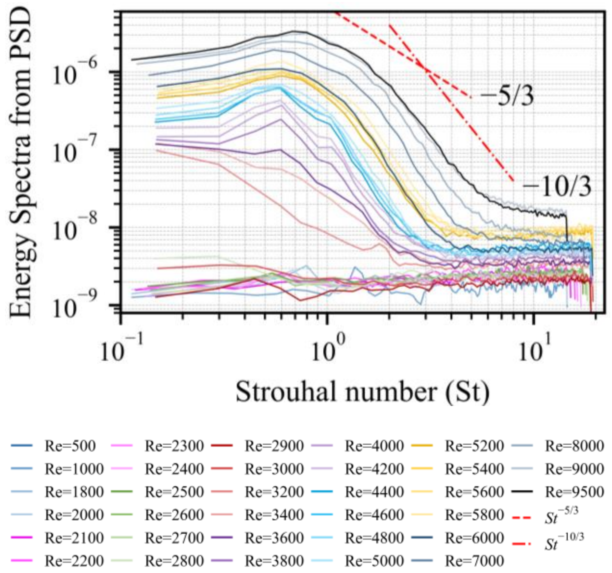

Figure 3: PSD of radial velocity magnitude measured with PIV and extracted in the centre of the cross-section as function of the Strouhal number for δ = 0.085.

Kolmogorov Scales

Even though the Kolmogorov time scale (Eq. 6) is no marker for transition, its trend can illustrate the differences between the laminar and turbulent flow states and is presented in Figure 4.

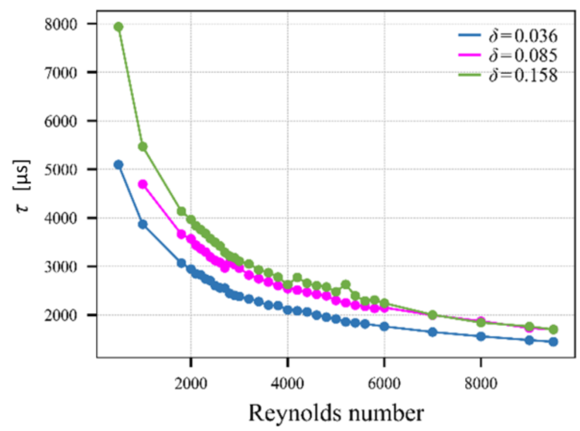

Figure 4: Kolmogorov time scale as function of the Reynolds number for the three curvature ratios.

It decays exponentially with rising Reynolds number since eddies become smaller and decay faster with increasing turbulence. Because of that, it is also an important measure for the calculation of the Spectral Entropy. According to Abdelsamie et al. (2017) the Spectral Entropy Method works best with a time-step in between consecutive snapshots of $[\tau_\eta; 2\tau_\eta]$ where the images become independent of each other. For a first approximation, every N = 300 images are taken for each set as input for the Spectral Entropy, resulting in time steps between two consecutive images of t_{step} = 0.03 … 0.6 seconds depending on the recording rate.

Spectral Entropy

The Spectral Entropy (SE) marks the laminar-turbulent transition by its value: while small SE values mark laminar flow, high SE means turbulence, the transition region in between is characterised by a strong slope.

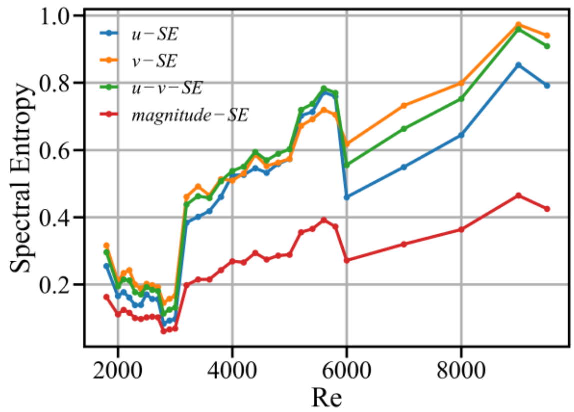

Figure 5: Spectral Entropy of δ = 0.085 as function of the Reynolds number.

Figure 5 shows the spectral entropy of δ = 0.085 for both single velocity components *u* and *v*, the *u*-*v* plane and the velocity magnitude. All curves show the same trend with a strong increase at Re = 3200 similar to the other markers indicating the onset of turbulence. The SE of the *u*-*v* plane lies between the two single component curves. The SE of the velocity magnitude is about half the values of the other curves, because only the amplitude of the velocity vector is considered in the correlation, but not the velocity direction. As a marker for turbulence, the spectral entropy of the full measurement *u*-*v* plane seems the most appropriate, since it contains all measured velocity information. These results are compared in Figure 6 for all three geometries.

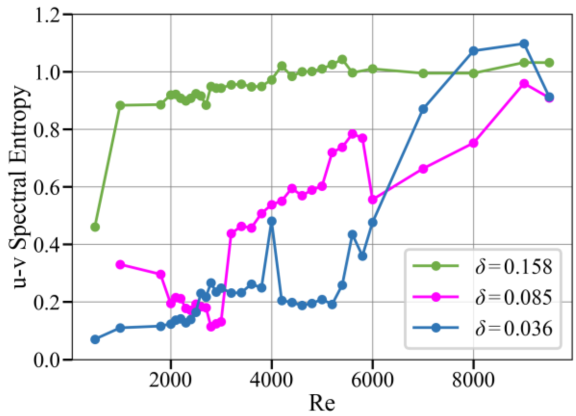

Figure 6: Spectral Entropy of the *u*-*v* plane as function of the Reynolds number.

The SE values increase with the onset of turbulence at Re = 500, 3200 and 5400 for the three curvature ratios respectively. The formation of a steady plateau indicates the end of the transition region and thus fully developed turbulence with an SE value of SE ≈ 1, which is reached for δ = 0.158 around Re = 4000, for δ = 0.0.036 at Re = 8000 and just about to be reached for δ = 0.085 at Re = 9000.

CONCLUSIONS

In this study the laminar-turbulent transition in three helix reactors with different curvature ratios ($\delta = 0.158$, 0.085 and 0.036) was examined and the results are presented for different turbulence markers including the newly employed Spectral Entropy Method.

The Spectral Entropy is able to capture the laminar-turbulent transition in the experimental data very accurately when compared to conservative markers. However, the experimental uncertainties like measurement noise and also post-processing parameters can influence the absolute values of the SE. Therefore, the Reynolds number of strong slope changes of the curves seem to better indicate transition than an absolute value of SE, as originally prescribed by Abdelsamie et al. (2017).

The markers and resulting transition ranges presented in this work and shown by crosses in Figure 1 are comparable to results from literature, with the advantage of a very strong data base and a more comprehensive analysis due to the use of multiple markers resolving the flow temporally and spatially.

OUTLOOK

Future work should include longer measurement durations with low speed PIV to ensure independent snapshots for the Spectral Entropy calculation based on the Kolmogorov time scale which was here estimated by the dissipation rate. However, low speed PIV can then not be interpreted with the conservative markers due to the too low temporal resolution.

Acknowledgments

The experimental equipment has been funded by the Deutsche Forschungsgemeinschaft (DFG, German Research Foundation) under grant number 444994527.

The authors would like to thank Pauline Nikoleizig and Amal Kootala for their help and support with carrying out the measurements and Pauline Nikoleizig for her help with the processing.

REFERENCES

Abdelsamie, A., Janiga, G., & Thévenin, D. (2017). Spectral entropy as a flow state indicator. *International Journal of Heat and Fluid Flow, 68*, 102-113. doi:10.1016/j.ijheatfluidflow.2017.09.013

Cioncolini, A., & Santini, L. (2006). An experimental investigation regarding the laminar to turbulent flow transition in helically coiled pipes. *Experimental Thermal and Fluid Science, 30*(4), 367-380. doi:10.1016/j.expthermflusci.2005.08.005

Eustice, J. (1910). Flow of water in curved pipes. *Proceedings of the Royal Society of London. Series A, Containing Papers of a Mathematical and Physical Character, 84*, 107-118. doi:10.1098/rspa.1910.0061

Eustice, J. (1911). Experiments on Stream-line motion in curved pipes. *Proceedings of the Royal Society of London. Series A, Containing Papers of a Mathematical and Physical Character, 85*, 119-131. doi:10.1098/rspa.1911.0026

Hart, J., Ellenberger, J., & Hamersma, P. J. (1988). Single and Two Phase Flow through helically coiled tubes. *Chemical Engineering Science, 43*, 775-783. doi:10.1016/0009-2509(88)80072-1

Itó, H. (1959). Friction Factors for Turbulent Flow in Curved Pipes. *Journal of Basic Engineering*, 123-132. doi:10.1115/1.4008390

Itó, H. (1987). Flow in curved pipes. *JSME International Journal, 30*. doi:10.1299/jsme1987.30.543

Kraichnan, R. H., & Montgomery, D. (1980). Two-dimensional turbulence. *Rep. Prog. Phys., 43*. doi:10.1088/0034-4885/43/5/001

Kubair, V., & Varrier, C. B. S. (1962). Pressure drop for liquid flow in hellical coils. *Transactions of the Indian Institute of Chemical Engineers*, 93-97.

Kühnen, J., Braunshier, P., Schwegel, M., Kuhlmann, H. C., & Hof, B. (2015). Subcritical versus supercritical transition to turbulence in curved pipes. *Journal of Fluid Mechanics, 770*. doi:10.1017/jfm.2015.184

Kühnen, J., Holzner, M., Hof, B., & Kuhlmann, H. C. (2013). Experimental investigation of transitional flow in a toroidal pipe. *Journal of Fluid Mechanics, 738*, 463-491. doi:10.1017/jfm.2013.603

Li, Y., Guan, Z., Zhao, H., & Zhuang, N. (2025). Numerical study of flow evolution and secondary flow dynamics in helical coils with periodically varying curvature. *Annals of Nuclear Energy, 223*. doi:10.1016/j.anucene.2025.111651

Mandal, M. M., Aggarwal, P., & Nigam, K. D. P. (2011). Liquid–Liquid Mixing in Coiled Flow Inverter. *Industrial & Engineering Chemistry Research, 50*(23), 13230-13235. doi:10.1021/ie2002473

Mansour, M., & Thévenin, D. (2023). Germany Patent No. EP19176360NWB1. European Patent Office: O.-v.-G.-U. Magdeburg.

Mishra, P., & Gupta, S. N. (1978). Momentum Transfer in Curved Pipes 1. Newtonian Fluids. *Ind. Eng. Chern. Process Des. Dev., 18*.

Müller, C., Kováts, P., Thévenin, D., & Zähringer, K. (2025). *Laminar - turbulent transition in helically coiled reactors. An experimental study with high-speed PIV.* Paper presented at the 19th International Conference on Fluid Flow Technologies (CMFF'25), Budapest, Hungary.

Müller, C., Kováts, P., Thévenin, D., & Zähringer, K. (2026). Laminar-turbulent transition in helically coiled reactors: An experimental study using high-speed PIV and LDV. *Experiments in Fluids, [IN REVISION]*.

Naphon, P., & Wongwises, S. (2006). A review of flow and heat transfer characteristics in curved tubes. *Renewable and Sustainable Energy Reviews, 10*(5), 463-490. doi:10.1016/j.rser.2004.09.014

Narasimha, R., & Sreenivasan, K. R. (1979). Relaminarization of Fluid Flows. In (pp. 221-309).

Pope, S. B. (2000). *Turbulent flows*: Cambridge University Press.

Schmidt, E. F. (1967). Warmeubergang und Druckverlust in Rohrschlangen. *Zeitschrift fur Technische Chemie, Verfahrenstechnik und Apparatewesen, 39*, 781-832.

Sigalotti, L. D. G., Alvarado-Rodríguez, C. E., & Rendón, O. (2023). Fluid Flow in Helically Coiled Pipes. *Fluids, 8*(12). doi:10.3390/fluids8120308

Sreenivasan, K. R., & Strykowski, P. J. (1983). Stabilization effects in flow through helically coiled pipes. *Experiments in Fluids, 1*, 31-36. doi:10.1007/BF00282264

Vashisth, S., Kumar, V., & Nigam, K. D. P. (2008). A Review on the Potential Applications of Curved Geometries in Process Industry. *Ind. Eng. Chem. Res., 47*, 3291-3337. doi:10.1021/ie701760h

Yanase, S., Yamamoto, K., & Yoshida, T. (1994). Effect of curvature on dual solutions of flow through a curved circular tube. *Fluid Dynamics Research, 13*, 217-228. doi:10.1016/0169-5983(94)90050-7